A SPAD-based Visible Light Communications Receiver Employing Higher Order Modulation

A SPAD-based Visible Light Communications Receiver Employing Higher Order Modulation

Oscar Almer*, Dobroslav Tsonev*, Neale A. W. Dutton*†, Tarek Al Abbas*, Stefan Videv*, Salvatore Gnecchi*†, Harald Haas*, Robert K. Henderson*

*School of Engineering, The University of Edinburgh †STMicroelectronics Imaging Division, Edinburgh, UK

***Abstract*—This paper studies complex modulation schemes, including orthogonal frequency-division multiplexing (OFDM), received by a single photon avalanche diode (SPAD) array integrated circuit (IC). A SPAD operates in the Geiger mode, and is able to detect single photons. This feature enables order of magnitude receiver sensitivity in intensity modulation (IM) / direct detection (DD) Visible Light Communication (VLC) systems. The tradeoff between received power and bit error ratio (BER) using both pulse-amplitude modulation (PAM) and OFDM is shown. A first order model of the noise in a digital SPAD receiver is derived. The noise in the experimental receiver chip approaches the predicted noise in our model, and we achieve receiver sensitivity of -64 dBm with a 100 kbit/s signal at a BER of 10^{-5}. It is concluded that future improvements in SPAD VLC receiver architecture will allow sensitivity to approach the quantum limit.**

I. Introduction

VLC uses the visible spectrum to transmit high speed data as well as to provide illumination at the same time. SPADs are used in applications where single photon sensitivity and picosecond resolution of the time of arrival of light are important considerations, such as scientific imaging [1], imaging of ultra-fast optical phenomena (such as light in flight) [2], and combined imaging and laser range-finding [3]. SPADs have also been used for VLC communications before [4], [5], but this is the first experimental demonstration of SPAD receivers for VLC with higher order modulation.

In this paper we present a model of the noise introduced into an optical communications channel by a SPAD sensor and the effect of the noise on PAM and OFDM with Quadrature Amplitude Modulation (QAM). We further present an evaluation of using a specific SPAD sensor as a receiver for VLC, and particularly note that the sensitivity achieved (-64 dBm at 10^{-5} BER and 100 kbit/s) is close to the state of the art APD designs, by observing that a factor of 10 in data rate requires an additional 10 dBm of signal power (6). Current APD designs achieve -31.8 dBm at 1 Gbit/s [6] to -29.9 dBm at 10 Gbit/s [7], and the closest APD used for VLC at -38 dBm at 310 Mbit/s and a BER of 3×10^{-9} [8], albeit at higher data rates. In this paper we present reception of 2-PAM and 4-PAM modulated data as well as novel reception of 2-QAM, 4-QAM, 8-QAM and 16-QAM OFDM modulated data, and present BER evaluations for these modulation schemes. In addition we show that the performance of the experimental sensor is not at the quantum limit, and that further improvement can be made in this regard to increase sensitivity. We discuss improvements to the receiver design and provide a future outlook on the use of the technology in VLC.

This paper is divided into Section II which discusses the SPAD technology and the particular IC that we use, and also develops our first-order noise model. Section III then introduces the experimental setup and the imperfections in the receiver that affects our results. In Section IV we show the obtained data and show working reception of complex modulation schemes. We finally give concluding remarks in Section V.

This work was supported by the Engineering and Physical Sciences Research Council through the Ultra-Parallel Visible Light Communications Project under Grant UP-VLC EP/K00042X/1. We are grateful to STMicroelectronics for chip fabrication.

II. Background

In this section we discuss the background to our work. We introduce SPAD arrays and the particular chip we use for our experiments as well as the noise models we use in our experiments.

A. SPAD arrays

A SPAD is a reverse-biased avalanche photo-diode with the dual advantages of single photon sensitivity and picosecond temporal resolution. The key advantage of SPAD receivers is in the very high detector gain, resulting in detector sensitivity approaching the photon shot noise limit. A SPAD produces a voltage pulse with every photon, after which it enters a dead time where it is insensitive to incoming light before it can be triggered again. The length of the dead time depends on the size and quench type of the SPAD devices. Actively quenched SPADs have controllable dead time whereas passively quenched SPADs do not [9], [10]. For our SPADs the dead time is in the region of 30-60 ns, dependant on manufacturing factors. Several SPADs simultaneously paralysed by dead time is referred to as pile-up distortion. Combining SPADs in an array through a timing balanced tree has been shown in an analogue Silicon Photo Multiplier (aSiPM) or through digital SiPM (dSiPM) to mitigate detection pile-up distortion [11]. A SPAD also have a dark count rate, which is the rate at which the SPAD pulses despite not being hit with any photon, caused by the intrinsic shot noise in the device.

In a SPAD receiver some rapid means of summation is required to reach a high sample rate. The stream of summed photon counts provides a digital representation of the optical signal. An XOR tree is a hardware efficient summation approach providing maximum linearity and dynamic range,

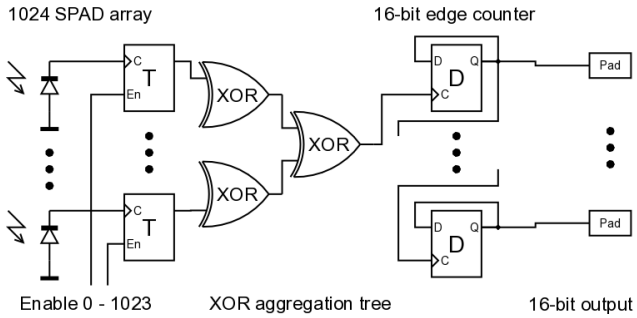

Fig. 1: Simplified schematic of the SPAD array chip. From [13].

but there are also other methods of summation such as an OR tree or adder tree. Hardware efficient summation is a key requirement for optically efficient SPAD receivers as electronic hardware occupies an area more usefully devoted to gathering light and improving receiver sensitivity. The percentage loss of optical signal in this way is referred to as the receiver fill-factor (FF).

B. SPAD array chip

In this paper, we present the single photon counting performance for 2-PAM and 4-PAM as well as OFDM VLC applications of a SPAD-based IC comprising of a 43% fill factor 32×32 SPAD array, a novel XOR based aggregation tree and single channel 16 bit ripple counter. The sensor was originally described for Time of Flight (ToF) applications in [12]. Fig. 1 shows a simplified schematic of the chip. Each SPAD in the 32×32 array is attached to a T-type flip-flop that toggles with each SPAD pulse in an asynchronous fashion encoding counts on both rising and falling edges of the output pulse. The output from the T-type is fed to an XOR aggregation tree, so that 1024 pixel outputs are combined into a single pulse stream recorded by an asynchronous high-speed 16-bit ripple counter. The 16 bit counter output is connected in parallel to 16 output pads for off-chip data transmission

Furthermore, each SPAD has a memory element, addressable externally, which connects or inhibits the SPAD output from connection to the XOR tree and thus prevents the SPAD from contributing to the count. This permits us to specify which SPADs combine to form the total count, allowing us to set the total active receiver area as another variable in our experiments.

C. PAM Noise Modelling

The combination of ambient light and SPAD dark count rate set the minimum intensity level that can be received and decoded. If the received signal is lower in intensity than the ambient or is below the total receiver dark count rate, it becomes difficult to distinguish the signal.

For a N-level PAM scheme, we define received average photon count for each of the levels as $n_1 ... n_{\max}$. We note that n_1, which is customarily associated with the 'all-zeroes' transmission state, is by necessity equal to or above the dark count rate for the SPAD array multiplied by the number of SPADs active in the whole array, or equal to or above the ambient light level per unit time. Additionally, $n_{\max}$ is also influenced by the number of SPADs in the array, but the calculation here is more complex as it depends on several other architectural factors of the array. We do not assume the photon levels $n_1 ... n_{\max}$ to be equidistant, as some factors in the design of SPAD arrays, and particularly in the design of the circuitry for combination of SPAD counts, influence the spacing between levels.

We model the noise in the SPAD array receiver as photon shot noise limited. The inherent dark count rate noise in a SPAD sensor is Poisson-distributed due to the nature of the sensor. Therefore, the OOK (2-PAM) BER models have the form:

$$\mathrm{BER} = \frac{1}{2}\sum_{k=th}^{\infty}\frac{n_1^k}{k!}e^{-n_1} + \frac{1}{2}\sum_{k=0}^{th}\frac{n_2^k}{k!}e^{-n_2} \tag{1}$$

given th as the optimal decoding threshold and n_1, n_2 received photon levels for 0 and 1, respectively. In addition, Poisson distributed variables can, via the central limit theorem, be well approximated by a Gaussian distribution with mean and variance both equal to n. In our treatment we do not make use of this property so as to simplify the problem.

As the Poisson distribution does not have a separate mean and variance, we can determine th analytically by finding the intercept between the two distributions:

$$\frac{n_1^{th}}{th!}e^{-n_1} = \frac{n_2^{th}}{th!}e^{-n_2} \tag{2}$$

$$th = \frac{n_1 - n_2}{\log(n_1) - \log(n_2)} \tag{3}$$

Optimal detection is achieved by setting the threshold at the minimal point which is determined solely by the photon levels in the received signals. This can be performed dynamically with only a small overhead in a receiver and still yield optimal detection.

D. 4-PAM noise modelling

We model the Poisson noise introduced in the the SPAD array receiver assuming a noiseless channel. For 4-PAM we define received photon levels $n_1 ... n_4$ and thresholds $t_1 ... t_3$.

$$\begin{aligned}\mathrm{BER} = \\ &\frac{1}{4}\sum_{k=th_1}^{\infty}\frac{n_1^k}{k!}e^{-n_1} + \frac{1}{4}\left(\sum_{k=0}^{th_1}\frac{n_2^k}{k!}e^{-n_2} + \sum_{k=th_2}^{\infty}\frac{n_2^k}{k!}e^{-n_2}\right) \\ &+ \frac{1}{4}\left(\sum_{k=0}^{th_2}\frac{n_3^k}{k!}e^{-n_3} + \sum_{k=th_3}^{\infty}\frac{n_3^k}{k!}e^{-n_3}\right) + \frac{1}{4}\sum_{k=0}^{th_3}\frac{n_4^k}{k!}e^{-n_4}\end{aligned} \tag{4}$$

Just as in the OOK case, the thresholds can be determined from $n_1 ... n_{\max}$. To do so, we assume the probability that a symbol moves more than one symbol level is negligible. We apply (3) three times to the pairs (n_1, n_2), (n_2, n_3) and (n_3, n_4), generating decoding thresholds th_1, th_2 and th_3 respectively.

	BER					
DCR	10^{-1}	10^{-2}	10^{-3}	10^{-6}	10^{-9}	10^{-12}
1	3.0	5.5	8.0	16.0	23.0	30.0
10	14.5	20.0	24.0	35.5	46.0	55.5
50	59.5	69.0	76.5	94.5	110.0	123.5
100	113.5	125.5	135.5	158.5	177.5	194.5

TABLE I: Numerical results relating the average signal level (in photons/bit) needed for receiving a 2-PAM signal given a BER and ambient photon rate.

	BER					
DCR	10^{-1}	10^{-2}	10^{-3}	10^{-6}	10^{-9}	10^{-12}
1	9.0	15.5	24.2	45.1	70.2	95.1
10	17.5	29.8	39.6	69.9	98.8	126.8
50	48.1	66.9	81.1	120.1	155.1	190.5
100	84.1	102.8	122.6	167.9	208.6	219.0

TABLE II: Numerical results relating the average signal level (in photons/bit) needed for receiving a 4-PAM signal given a BER and ambient photon rate. Note that this is per bit for 4-PAM and thus the photons per symbol is double the reported numbers.

E. Photons per bit

For 2-PAM and 4-PAM we can further determine the average number of photons required per received bit at a given BER. Assume we have a target BER, which can be expressed in terms of the average photons per level as per (1) and (4). The average number of photons per bit can clearly be seen to depend on two factors; the ambient light level / dark count rate and the required BER. The ambient light level dictates the level n_1 whereas the required BER will dictate the spacing to, and between, the other levels. Unfortunately rearranging (1) taking into account (3) to solve for n_2 in terms of n_1 and BER is difficult to perform analytically.

We present Table I and II that numerically gives the minimum average number of photons per bit, given a BER and an ambient level (in photons per sampling period). These tables are generated through limited search (as exhaustive search proved excessively time consuming) of the range $n_1 ... n_{\max}$, computing the BER as above. The limited search was performed by abandoning further iterations once it was clear that a better result could not be found by further increment of n_p.

F. Relating BER and incident light power

First-order receiver noise as a function of the received photon levels for 2-PAM and 4-PAM is given in (1) and (4). The received photon level in these equations is related as per (5) where E_l is the received power in W for each PAM level.

$$n_l \beta \frac{hc}{\lambda} = E_l t_\Delta \tag{5}$$

For this purpose we consider monochromatic light with wavelength λ and that the sampling period is t_Δ. β is a conversion factor that depends on the SPAD architecture, and is expressed as the probability of SPAD triggering given an incident photon of a given wavelength.

Reorganising, we can find a first order approximation of the sensitivity in dBm for a given BER in an ideal SPAD receiver. We use the maximum modulation light level here, as this gives the most pessimistic value for sensitivity. It is also possible to use the average photon counts, as well as n_1 to derive the ambient level.

$$E_{\max} = \frac{n_{\max} hc}{t_\Delta \lambda \beta} \tag{6}$$

For 2-PAM, the minimum received photon level per unit time required for receiving at 10^{-12} BER in darkness is 30, as stated in Table I. If we assume a perfect conversion factor, the ideal receiver would be capable of receiving 2-PAM 1 Mbit/s signals down to -79 dBm signal power. At that power and rate the receiver is quantum limited and cannot reasonably be improved further. If we wish to improve the data rate to 1 Gbit/s we arrive at a minimum signal level of -49 dBm.

Combining fill-factor and SPAD photon detection efficiency at the wavelength of interest, an approximation for $\beta = 0.2$ is made [14] and inserting this into (6) we arrive at a maximum sensitivity of -72 dBm using this SPAD receiver.

This does not take into account the light intensity per unit area (irradiance), for which we will also need to factor in the sensor active area. Irradiance is in units of W/m^2, and we can derive it from received photon counts as:

$$I_{\max} = \frac{n_{\max} hc}{t_\Delta \beta \lambda A_{\text{spad}}} \tag{7}$$

Relating this to Eqns. (1) allows us to find a level of irradiance that can support a given modulation.

G. OFDM noise

We note that the sub-carrier noise in OFDM will be Gaussian even for a non-Gaussian channel [15]. Due to the FFT transform, the noise distribution in the QAM constellations do not significantly differ from Gaussian, and there is therefore no need to derive the effects of shot noise limited receiver for OFDM.

III. Experimental setup

Our setup is a model for the case where a VLC transmitter (e.g. a light bulb) is the dominant source of illumination in an area. The SPAD IC we are using is illuminated by an off-the-shelf 520 nm wavelength LED (Multicomp OVL-3324) placed at 15 cm distance from the sensor in darkness. The LED is driven by an Agilent 33220A arbitrary waveform generator (AWG) under computer control. Performing the experiment in darkness ensures that background light sources (e.g. sunlight or flicker from mains lighting) are minimised and the dominant noise source is solely the SPAD receiver dark count. The output of the SPAD receiver IC is wired to a Xilinx Spartan6 FPGA with specialised firmware for handling data capture and streaming to the control computer.

Both 2-PAM and 4-PAM waveforms, as well as 2 to 16 QAM OFDM waveforms, with randomly generated binary data sequences, are sent through the AWG. LED voltage levels are set such that the minimum LED light level generates a SPAD count above the dark count rate.

The recorded data sequence from the sensor is 2^{20} samples in length and stored in the PC alongside the original transmitted waveform for off-line post-processing. All experiments were carried out with the same SPAD array chip.

A. Design issues

The SPAD array used for these experiments was not primarily designed for VLC applications [12]. Due to this, several conclusions and design considerations are made to create an optimal SPAD-based receiver for VLC applications.

1) Cancellation: The architecture needs to minimise SPAD event cancellation. In the device used, SPAD event combination is done through a combinatorial XOR tree. While this is very space and energy efficient, as the number of SPAD events per unit time goes up, it suffers from increasing rate of cancellation, whereby two edges in the tree are so close together in time that they cancel out, leading to no photon being counted.

This effect is discussed in [13] and is there shown to cause nonlinear photon count saturation at around 600 photons / μs.

This saturation effect causes increased BER compared to the ideal case due to two complementary mechanisms: the saturation reduces the dynamic range directly, as we do not count all photons at high photon rates, and also introduces a non-linearity into the channel as the photon counting saturates.

2) Oversampling: Another cause of extra noise compared to the ideal case is that the 2's complement counter output from the SPAD array chip is asynchronous. The count updates whenever there is a SPAD event, which means it is not synchronous to any clock. This scheme, while simple, has two problems that affect the accuracy of the output.

The count rate in the SPAD array can reach several hundred photons / μs, which means that the chip output pins are switching at several hundred MHz, above the specifications for the pads on the chip to drive. This primarily affects the bottom bits in the output number, and means that we lose some precision in the number of SPAD events recorded. At the maximum recorded photon rate, where we can clearly see evidence that the bottom 3 bits are degraded. The effect is dependent on signal magnitude, and the precision is lost in the least significant bits when the signal level is high. We do not include this in the receiver noise treatment above as it is an effect particular to the SPAD array used and not an inherent artefact of SPAD arrays in general.

The other problem with the asynchronous output is that the data needs to be resynchronised to a clock. Therefore the custom FPGA design used to interface the chip contains a dedicated resynchronizer for each bit in the interface. As with all resynchronisers, this reduces the effect of the inherent metastability issues, but due to the 2's complement coding used and the data rates, it does occasionally introduce single-cycle bit errors. These events show up as a value excursion in the positive or negative direction, followed by an excursion of approximately the same size in the other direction in the subsequent clock cycle. In addition, when the 16-bit counter resets, it also appears as a large excursion in the difference waveform.

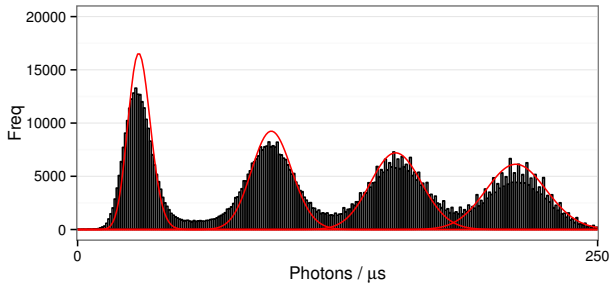

Fig. 2: 4-PAM histogram before median filtering. Poisson distributions generated from the means of the peaks are overlaid in red.

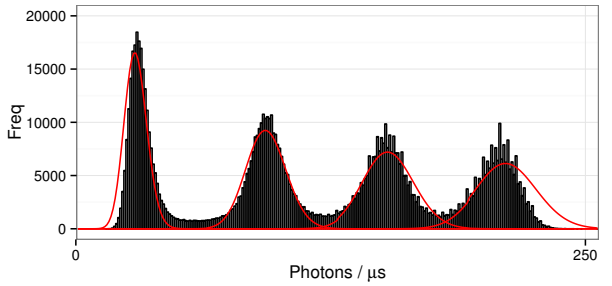

Fig. 3: 4-PAM histogram after median filtering. Poisson distributions of the peaks are overlaid in red. It is clear that the peaks have grown sharper through the median filtering.

To solve both these problems, which appear as random 'salt and pepper noise', we initially apply a length 5 median filter to the difference waveform to obtain our decodable waveform. This length is chosen as a shorter filter will not remove the double-errors which occur in the data stream. Due to the response of the median filter we cannot use symbol rates that are close to the sample rates of the system, but have to oversample in the receiver and then down-sample as appropriate after the median filter. Therefore we have used a up-sampling and down-sampling scheme in all experiments, so that each transmitted symbol is 10 samples in length.

Introducing the median filter has an unexpected side effect in that it significantly improves PAM detection as the median function reduces the variation in the oversampled symbol. As seen in Figs. 2 and 3 this is because the filter combined with the 10$\times$ oversampling increases the height of the peaks in the signal histogram by removing outliers in the data. The BER formula predicts that the received waveform in Fig. 2 should have a BER of 1.1×10^{-2} but in fact the waveform in Fig. 3 is the one detected, and the achieved BER in doing so is 9×10^{-4}.

B. PAM format

We construct PAM frames with two repeating, regular, pilot sequences of 100 symbols each. These are followed by 2000 symbols of random data. Each symbol encodes 1 bit (2-PAM) or 2 bits (4-PAM). The resultant modulated waveform is up-sampled by a factor of 10 before transmission. We transmit the waveform, in different experiments, at 1 Msample / s or 10 Msamples / s, corresponding to 100 kbit or 1 Mbit nominal

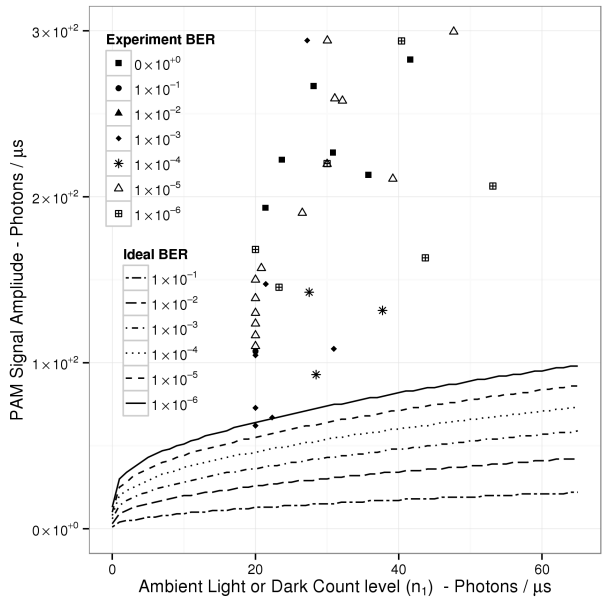

Fig. 4: Theoretical maximum BER versus obtained BER in terms of photons per bit for 2-PAM. The theoretical maximum BER is plotted as lines whereas the experimentally obtained BER is inserted as points.

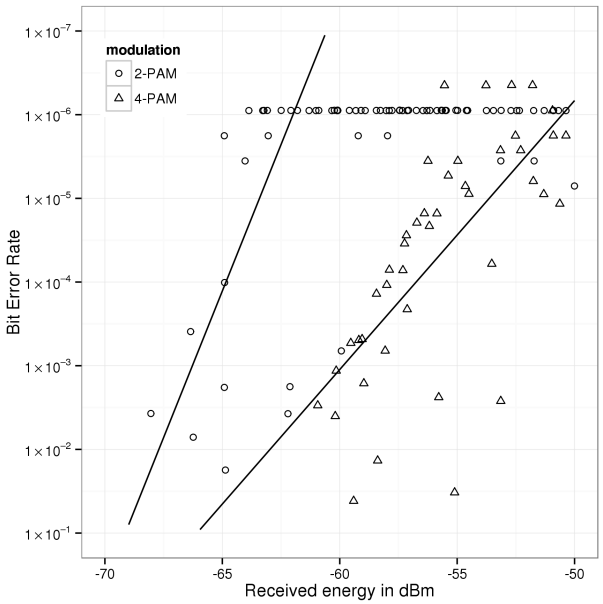

Fig. 5: Obtained BER plotted against obtained dBm for 100 kS / s PAM. The general trend is for decreasing BER with received energy, but this is moderated by several factors such as number of SPADs used and non-linearity in the transmitter. Trends drawn in are for 2-PAM (left) and 4-PAM (right).

data rates. Actual data rates are lower due to the pilot symbols and inter-frame time.

The receiver locates each PAM frame in the received waveform through cross-correlation with the known pilot waveform. The received data is then extracted by taking the next 200,000 samples. Decoding uses the method developed in Section II-C for finding peaks in received histograms, and from there develops the optimal thresholds $th_1 ... th_{\max}$. These are used in a hard decision decoder which looks for the centre parts of the oversampled waveform to reduce the bit error rate.

C. OFDM Format

For OFDM we found it necessary to linearize the channel to remove some of the nonlinear effects in the channel, including the saturation nonlinearity discussed in III-A1. We linearized through a closed loop method, where the test setup generated correction factors based on a received waveform.

We transmit OFDM frames consisting of 2 pilot frames and 21 data frames. The pilot frames are identical and contain random data that is assumed to be known in the receiver. The data frames consist of unknown randomly generated data. Each sub-carrier in the OFDM frame is QAM modulated, using QAM with 2 though 16, using standard grid constellations. Each frame has 512 sub-carriers, chosen as a middle ground value, and we use the real-valued IFFT outputs obtained through using the complex conjugate together with the normal data in the transmitter. A cyclic prefix of 4 samples is added to each frame transmitted. The resultant real waveform is up-sampled and filtered by a factor of 5 before transmission due to the receiver design issues discussed in Section III-A. In addition, we clip the waveform to 3 standard deviations from the mean, so that large outliers do not affect the transmission resolution in the AWG.

As in the PAM case, we automatically locate the pilot sequence in the received complex through cross-correlation, and then extract the data frames from that index. In addition, we use the pilot frames (which are known in the receiver) to correct systematic sampling phase errors and magnitude errors. We apply the corrections to the data frames and then demodulate the result through the appropriate QAM hard decision demodulator. We also derive $n_{\max}$ for OFDM as the 3 standard deviation level from the mean.

IV. Results

In this section we discuss the results of a series of experiments using a SPAD array chip, and comparing the results to the theoretical limits established previously. We also discuss some practical limitations of the SPAD array used and offer some suggestions for improving the SPAD array design.

A. OFDM reception

Fig. 4 shows the theoretical BER calculated using the method given in Section II-E together with rates from experiments with out SPAD array chip. This figure shows that despite obtaining better BER rates than predicted, we have not, except in a few outlying cases, come close to the theoretical limits of a SPAD array receiver. This result is due to re-framing the bit error rate per photon received rather than per bit, and as we are using a 10 times oversampling the number of photons we receive is generally far larger than necessary for the bit rates obtained. In essence, due to the necessity of the median filter, we cannot use the full capacity of the receiver.

It should be noted that with the available sample sizes it has not been possible to measure BER rates above 10^{-6} as we only send and receive at most approximately 1.5 million

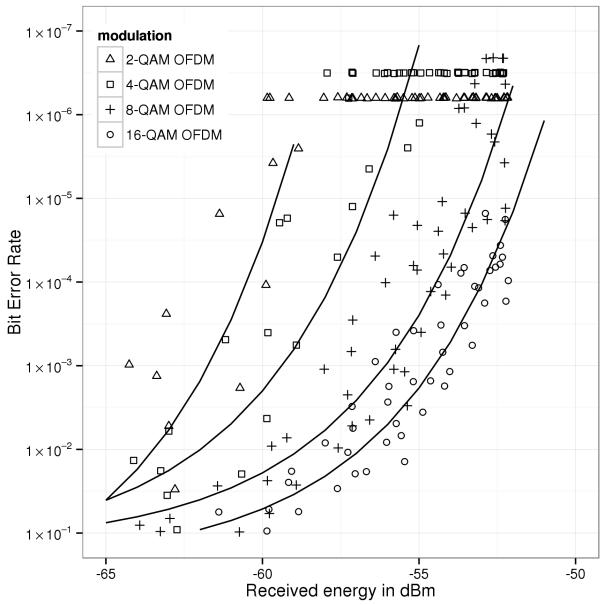

Fig. 6: Obtained BER plotted against obtained dBm for 200 kS / s OFDM. Exponential trendlines drawn in, from left to right: 2-QAM, 4-QAM, 8-QAM, 16-QAM. Clustering at top of graph is caused by experimental BER limit.

bits per experiment. Consequently, experimental BER rates of 10^{-5} should also be interpreted cautiously as they represent 10 bit errors in the entire experiment and that measurement therefore has low confidence.

B. Sensitivity

Our experiments show that we achieve a sensitivity of up to -64 dBm, without the use of any optical concentration, with bit error rates of at least 10^{-5} as shown in Fig. 5. In addition, in Fig. 6 we show reception of 2-QAM OFDM at -59 dBm and 8-QAM OFDM at -53 dBm, in both cases with the same bit error rate and a higher data rate of 200 kS / s.

These figures include the additional sources of noise discussed in Section III-A, and we are therefore not achieving the ideal of -72 dBm established in Section II-F. As we are oversampling by a factor of 10, we would expect to attain -62 dBm but we manage to achieve -64 dBm. We therefore conclude that the median filter effect corresponds to approximately an extra 2 dBm of sensitivity. This also shows that we are not limited by the inherent sensitivity of out SPADs, but are capable of better sensitivity with improved sensor IC architecture.

We also show in Fig. 5 that reception at the -68 dBm level is possible, though we do not realise the -72 dBm potential of the link computed earlier. Even so it is clear that a SPAD array receiver for VLC is capable of operating without appreciable optical gain, and the use of optical band-pass filtering and field of view restriction would provide additional gain in sensitivity by reducing ambient light.

V. Conclusions

SPAD arrays show significant promise for use in VLC applications due to the low inherent noise of SPADs. The design of the circuitry supporting the receiver array is critical, and the optimum SPAD VLC receiver design does not resemble that of other application for SPADs. With the limitations of the current detector architecture we achieve 100 kbit/s at -65 dBm and 3×10^{-5} BER.

The theoretically available sensitivity in SPAD array devices is higher than that available in APD sensors. We have not achieved significantly higher sensitivity then comparative APD devices in these experiments, but we have shown that it is possible to do so with improved sensor architecture. The downside with current generation SPAD arrays is that they cannot yet support the data rates possible in APD devices due to the dead time of a SPAD sensor. Increasing the available data rates is a question of increasing the array size rather than an intrinsic device issue, and as such we expect higher data rate SPAD receivers in the future.

References

[1] J. Richardson, R. Walker *et al.*, "A 32×32 50ps resolution 10 bit time to digital converter array in 130nm CMOS for time correlated imaging," in *Custom Integrated Circuits Conference, 2009. CICC '09. IEEE*, Sept 2009, pp. 77–80.

[2] G. Gariepy, N. Krstajic *et al.*, "Single-photon sensitive light-in-flight imaging," *Nat Commun*, vol. 6, Jan 2015, article. [Online]. Available: http://dx.doi.org/10.1038/ncomms7021

[3] C. Niclass, M. Soga *et al.*, "A 100-m range 10-frame/s 340×96-pixel time-of-flight depth sensor in 0.18-μm CMOS," *Solid-State Circuits, IEEE Journal of*, vol. 48, no. 2, pp. 559–572, Feb 2013.

[4] D. Chitnis and S. Collins, "A SPAD-based photon detecting system for optical communications," *Lightwave Technology, Journal of*, vol. 32, no. 10, pp. 2028–2034, May 2014.

[5] Y. Li, M. Safari *et al.*, "Optical ofdm with single-photon avalanche diode," *Photonics Technology Letters, IEEE*, vol. 27, no. 9, pp. 943–946, May 2015.

[6] P. Brandl, R. Enne *et al.*, "OWC using a fully integrated optical receiver with large-diameter APD," *Photonics Technology Letters, IEEE*, vol. 27, no. 5, pp. 482–485, March 2015.

[7] E. Yagyu, E. Ishimura *et al.*, "Design and characteristics of guardring-free planar AlInAs avalanche photodiodes," *Lightwave Technology, Journal of*, vol. 27, no. 8, pp. 1011–1017, April 2009.

[8] D. O'Brien, R. Turnbull *et al.*, "High-speed optical wireless demonstrators: Conclusions and future directions," *Lightwave Technology, Journal of*, vol. 30, no. 13, pp. 2181–2187, July 2012.

[9] L. Pancheri and D. Stoppa, "Low-noise CMOS single-photon avalanche diodes with 32 ns dead time," in *Solid State Device Research Conference, 2007. ESSDERC 2007. 37th European*, Sept 2007, pp. 362–365.

[10] S. Isaak, M. Pitter *et al.*, "Design and characterisation of 16x1 parallel outputs SPAD array in 0.18 um CMOS technology," in *Circuits and Systems (APCCAS), 2010 IEEE Asia Pacific Conference on*, Dec 2010, pp. 979–982.

[11] J. Arlt, D. Tyndall *et al.*, "A study of pile-up in integrated time-correlated single photon counting systems," *Review of Scientific Instruments*, vol. 84, no. 10, p. 103105, 2013.

[12] N. A. W. Dutton, S. Gnecchi *et al.*, "A time-correlated single-photon-counting sensor with 14GS/s histogramming time-to-digital converter," *Proceedings of the International Solid State Circuits Conference*, pp. 15–17, February 2015.

[13] O. Almer, N. A. W. Dutton *et al.*, "4-PAM visible light communications with a XOR-tree digital silicon photomultiplier," in *Photonics Society Summer Topical Meeting Series, IEEE*, July 2015.

[14] E. Webster, L. Grant *et al.*, "A high-performance single-photon avalanche diode in 130-nm cmos imaging technology," *Electron Device Letters, IEEE*, vol. 33, no. 11, pp. 1589–1591, Nov 2012.

[15] M. Safari, "Efficient optical wireless communication in the presence of signal-dependent noise," in *Proceedings of the IEEE International Conference on Communication*, June 2015.